

# Numerical and experimental analysis of the wake behavior of a generic submarine propeller

Fabio Di Felice<sup>1</sup>, Mario Felli<sup>1</sup>, Mattias Liefvendahl<sup>2</sup>, Urban Svennberg<sup>2</sup>

<sup>1</sup> Italian Ship Model Basin (INSEAN), Rome, Italy

<sup>2</sup> Swedish Defence Research Agency (FOI), Stockholm, Sweden

## ABSTRACT

The performance and fluid dynamics of a submarine propeller, running in open water conditions, was investigated using experimental and computational methods. The flow velocity was measured using Laser Doppler Velocimetry (LDV) and it was computed using Large Eddy Simulation (LES). The wake dynamics were investigated mainly by studying the velocity field in three transversal planes of the wake, at three loading conditions. The experimental results were also used to validate the accuracy of the simulations for the most important flow features.

## Keywords

Propeller, LES, LDV, wake instability, turbulence

## 1 INTRODUCTION

Acoustic signature reduction in a submarine is correlated to the design of the propulsive system mostly, propeller emitted noise being 30-50 dB higher than the other sources typically and, unlike them, having a spectrum dominated by specific tonal contributions (Felli and Di Felice, 2008). Submarine propeller noise is mainly the consequence of tip and hub vortex vorticity fluctuations induced by both the pronounced unsteady nature of the blade load, due to flow distortions of the upstream wake, and the periodic impact of vortical structures against the blades (i.e. bilge vortices, rudder horseshoe vortices, corner vortex originating in the hull-sail intersection region). The requirements to minimize propeller induced noise and vibrations have oriented submarine propeller designers towards complex configurations of the blade system, in order to minimize the blade load gradients along the azimuth as well as to avoid any coupling with the perturbation induced by the incoming flow. More specifically, a typical approach is the adoption of high blade number and highly skewed blades with tip unloading design. This solution allows high efficiency while reducing the size and the speed of the propeller and to minimize the contribution at the blade rate frequencies, by not having the entire leading edge hit the wake shadow at the same time. Moreover, blade trailing wake undergoes a large deformation, moving the interaction point between consecutive spirals closer to the propeller plane as compared to a conventional propeller (Di Felice

et al., 2004; Felli et al., 2008). Such an increased complexity of the propeller blade geometry has enhanced the interest towards detailed investigation tools of the propeller flow field. The present study deals with the investigation of the wake evolution mechanisms of a generic isolated free-running 7-bladed submarine stock propeller through both experimental and numerical approaches. The computations were carried out using LES and the results were validated against the experimental results, both quantitatively and qualitatively. Comparisons were made for the propeller performance, as well as the velocity field in the near wake. The LES results also provide information about the flow field around the blades where it is difficult to measure. Experiments were carried out in the INSEAN large Circulating Water Channel and concerned LDV measurements of the velocity distribution in three cross-planes of the wake at three values of the advance ratio. Velocity measurements were phase-locked with the propeller blade. The propeller geometry is presented in §2. The experimental set-up and the computational model are described in §3 and §4 respectively. Results are documented in §5. The results of the experiments and the simulations are compared and evaluated in §6. Then a brief summary is given in §7.

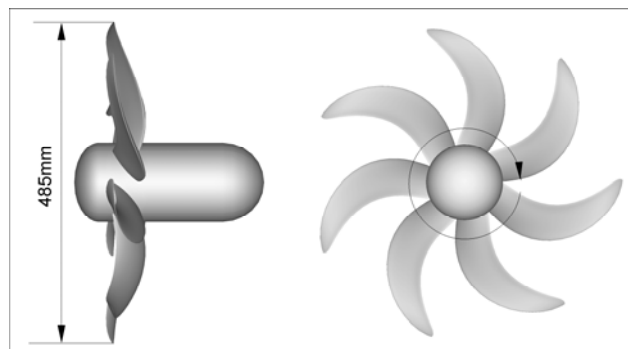


Figure 1. Geometry of the INSEAN E1619 propeller.

## 2 PROPELLER MODEL

The propeller was the 7-bladed propeller model E1619, designed by INSEAN (Figure 1). The model was built in one single piece of aluminum alloy “avional” and

checked with a 6-dof CMM. The outer skin was black anodized to reduce laser beam reflection during the tests. The main features of the propeller are documented in Table 1.

**Table 1. Main propeller parameters.**

	Symbol	INSEAN E1619
Number of blades	Z	7
Diameter (mm)	D	485
Hub Diameter Ratio	$D_h/D$	0.226
Pitch at $r = 0.7 R$	P/D	1.15
Chord at 0.75R (mm)	$C_{0.75}$	6.8

### 3 EXPERIMENTAL SET UP AND TEST CONDITIONS

Flow velocity was measured by means of a two-component-back-scatter-LDV-system, consisting of a 5W Argon Laser, a 2-component underwater fiber optic probe, a 40 MHz Bragg cell for the velocity versus ambiguity removal and two TSI IFA 655 Doppler processors. The probe allowed measuring the axial and vertical components of velocity simultaneously in the test section fixed frame. In view of the axi-symmetry of the propeller inflow and the steady conditions of operation, when the measurement volume is located on the vertical radius, the axial and the vertical components correspond to the axial and the radial ones in the propeller moving frame respectively. Instead, locating the probe in the horizontal radius (y-axis), they represent the axial and the tangential ones. All the measurements in a circumference were accomplished without moving the LDV volume so that the measurement grid in a plane is obtained by only radial movements (Cenedese et al., 1985).

The LDV measurement volume was traversed with an accuracy of about 0.01 mm. Its initial reference position was fixed by means of a special hub tip, endowed with a hole, providing an accuracy of 1 mm along the optical axis and 0.5 mm in the perpendicular direction. The tunnel water was seeded with 10 $\mu$ m Titanium dioxide particles (TiO<sub>2</sub>). Phase sampling of the velocity signals was performed using a rotary 3600 pulse/revolution incremental encoder and a synchronizer; the latter provides the digital signal of the propeller position to the TSI RMR (Rotating Machine Resolver). The synchronization was given using the detection of the Doppler signal as trigger condition: each LDV sample, tagged with the blade angular position at the measurement time was arranged inside angular slots and then processed statistically (see Stella et al., 2000 and Felli et al., 2005 for further details). Data acquisition was accomplished by using a standard PC. Velocity measurements were performed at the facility speed  $U_\infty=1.68$  m/s changing the propeller speed to get the values of the advance ratio  $J=0.65$ ,  $J=0.74$  and  $J=0.85$ .

### 4 COMPUTATIONAL METHODS

The flow solver has been developed at FOI, using the open source library OpenFOAM<sup>1</sup>, version 1.3. The OpenFOAM software library is designed to provide a high-level, object-oriented framework for the implementation of programs for the solution of coupled transport equations in general, and CFD in particular. The discretization of the governing equations is based on the Finite Volume Method (FVM). The FOI-solver which have been used in the present study, implements the LES model by Schumann (1975). The choice of LES model is not critical for simulation of the flow around the blades, and in the (very) near wake, since the flow in this region does not contain large turbulent regions, but is rather dominated by structures such as tip vortices and blade wakes. Wall modeling based on the law-of-the wall is applied next to boundaries where the no-slip condition is applied. The equations are solved on a rotating mesh, i.e. the equations are not transformed to a rotating frame of reference. The application of this methodology to propeller flows have been extensively tested before, and it is described in detail in Bensow and Liefvendahl (2008) and Bensow et al. (2006).

We use a cylindrical computational domain with the following dimensions.

$$-2.06 < x/R < 5.15 \quad r/R < 3.09$$

Here R is the propeller radius and x is the axial coordinate, which has the origin in the propeller plane and increases downstream. Mesh generation is a crucial practical aspect of propeller simulations. The tip-vortices and the blade wakes are very sharp flow features which require a fine mesh to be resolved. It is important to distribute the cells in a suitable manner in order to economize the number of cells, and thereby the computational cost. The main regions where a high mesh resolution is required are around the blades and in the near wake.

**Table 2. The number of cells in the two meshes - the coarse and the fine. The first row gives the total number of cells, while the second and third respectively give the number of tets and prims. The number N1 indicates the number of triangular surface elements used to represent a designated propeller blade. The last row shows the number of prismatic cell layers used on the propeller.**

	Coarse	Fine
<b>Total number of cells</b>	2 568 024	4 466 630
<b>Tetrahedral cells</b>	2 353 466	3 669 091
<b>Prismatic cells</b>	214 384	797 055
<b>N1</b>	8 158	16 766
<b>Prism layers</b>	3	5

Two computational grids have been constructed, with 2.6 and 4.5 Mcell (1 Mcell = 10<sup>6</sup> cells) respectively. The main part of the computational domain is meshed with tetrahedral (tet) cells and in the boundary layer a number

<sup>1</sup> [www.openfoam.com](http://www.openfoam.com)

of cell layers of prismatic (prism) type are inserted. The mesh around a blade is illustrated in figure 2. In table 2, we summarize the mesh characteristics.

It is a relatively common practice, at least for RANS simulations, to use the rotational symmetry (7-fold in the present case) of the propeller and only construct the mesh for a part of the domain which corresponds to one propeller blade. We note however that a study of the interaction between consecutive blade wakes, and the related wake instability, is excluded by the assumption that the flow field has the same symmetry as the propeller. The wake instability breaks the 7-fold symmetry, therefore we have constructed a mesh for the whole computational domain.

## 5 RESULT ANALYSIS

### 5.1 Performance characteristics

Open water propeller performance characteristics were analyzed both experimentally and numerically. Experiments were carried out in the INSEAN towing tank N.1 (i.e. 470m length, 13.5m width and 6.5m depth), using the special test rig for propellers Cussons R46 having 700N maximum thrust, 40Nm maximum torque and 2500 rpm maximum speed.

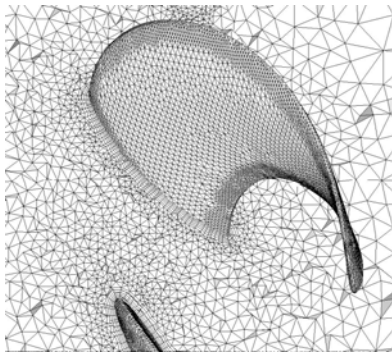


**Figure 2. Mesh on and around a blade. The surface mesh of the blade is shown as well as the volume mesh on a plane through the domain. The boundary layer mesh (with prism cells) can clearly be seen next to the blade.**

The average blade Reynolds number, referenced to the section at 70% of the radius, was about 230000. CFD analysis was performed by LES using 2 different mesh densities with 2.5M cells and 4M cells, at the advance ratios  $J=0.74$  and  $J=0.85$ . Results are documented in figure 3. It is seen that the numerical simulation well capture the propeller thrust and torque coefficients at both the values of the advance ratio. All computed values are within 5% of the measured values. We note that the simulation with coarse grid (i.e. 2.5 Mcells) is observed to be in slightly closer agreement with the experimental results. We believe however that this discrepancy can be explained by the unavoidable differences between the experimental and computational set-ups, which include: (1) Extent of flow domain. (2) Level and modeling of inflow turbulence. (3) Experimental procedure to find zero thrust. (4) Difference between computational grid representation of the propeller and the actual,

manufactured propeller. When carrying out an investigation, these types of differences should be minimized but they will always affect any comparison of results to some degree.

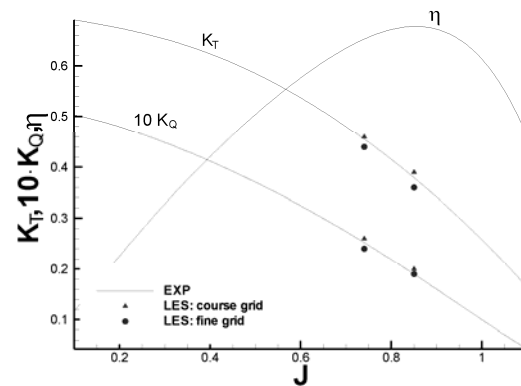


**Figure 3. Propeller performance characteristics.**

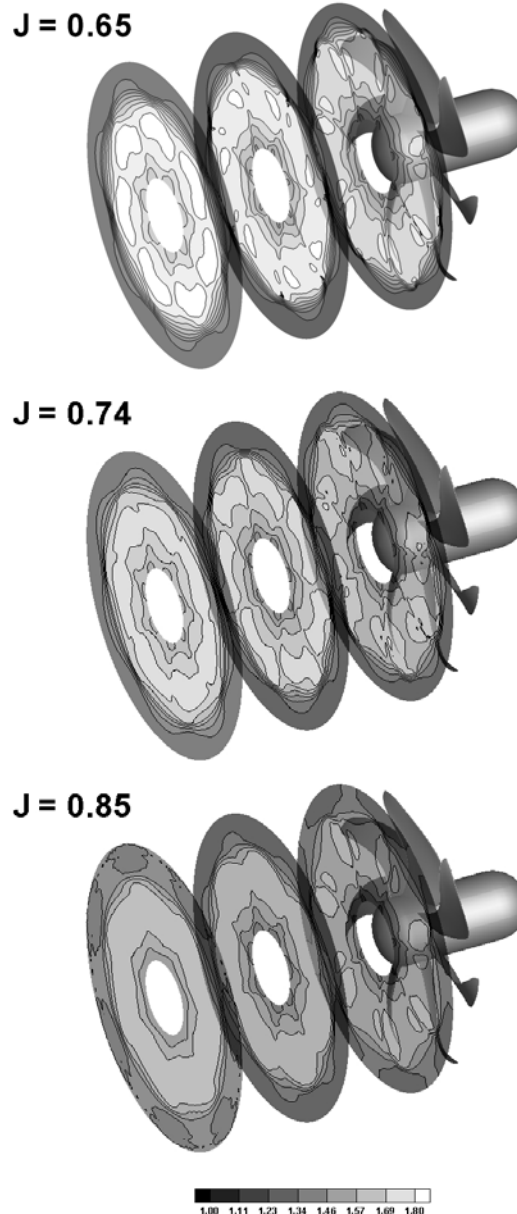


**Figure 4. Streamwise evolution of the axial velocity normalized with the facility speed (LDV measurements)**

## 5.2 Wake evolution

Propeller wake evolution was dealt with considering the distribution of the mean and fluctuating components of the velocity along three cross-sections of the wake at  $x=0.17R$ ,  $x=0.58R$  and  $x=R$ . The effect of the propeller loading condition on the wake features was investigated through the analysis of the velocity field at the advance ratios  $J=0.65$ ,  $J=0.74$  and  $J=0.85$ .

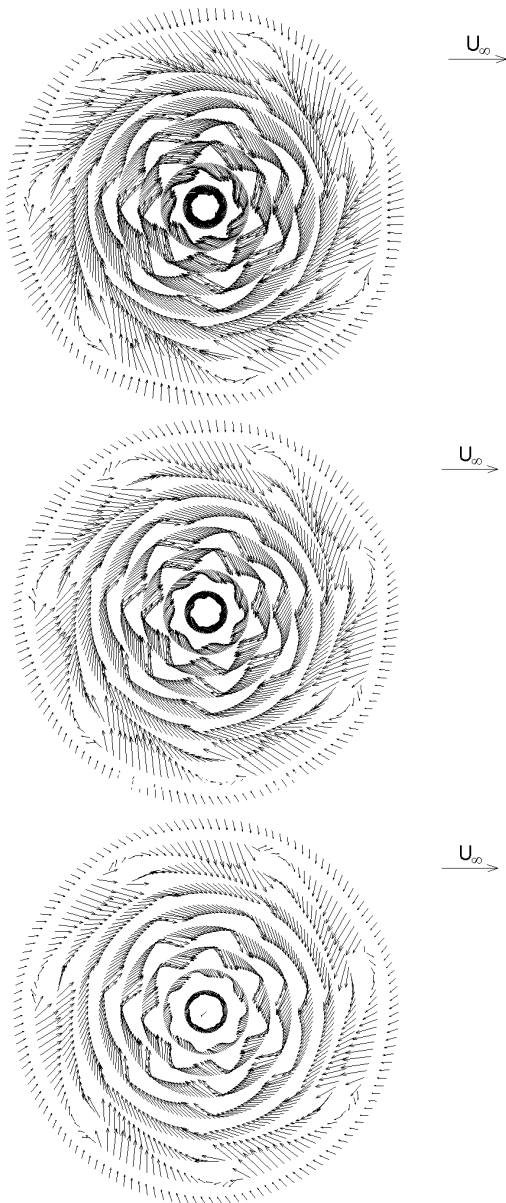


**Figure 5. Cross flow at  $x=0.17R$  for  $J=0.65$  (top),  $J=0.74$  (mid) and  $J=0.85$  (bottom) (LDV measurements)**

In the first plane (i.e.  $x=0.17R$ ), just downstream the blade trailing edge, a defect of axial velocity is observed due to the blade boundary layer and the momentum transfer from the axial to the cross components (Figure 4). The flow is mainly accelerated elsewhere with a maximum of the axial velocity on the suction side, at about  $r=0.75R$ , where the propeller is designed to develop maximum circulation. In the blade-to-blade area, both the intensities of the velocity defect and the rate of

acceleration show a dependence on the blade loading conditions. More specifically, the rate of acceleration  $U_{\text{disk}}/U_{\infty}$  (with  $U_{\text{disk}}$  the averaged axial velocity over the streamtube cross-section) in the first plane is about 60% at  $J=0.65$ , 50% at  $J=0.74$  and 40% at  $J=0.85$ . Radial and tangential gradients of the axial velocity become smoother more and more streamwise due to the rapid turbulent diffusion of the blade wake. The cross flow distribution is represented by the vector field in figure 5, limitedly to the section at  $x=0.17R$  for space reason. The cross flow velocity components show marked changes across the blade wakes. Outside the blade wakes, the radial flow is globally inward direct as the consequence of the wake contraction. Indeed, the intensity of such an inward radial component is reduces streamwise. Within the blade wake, flow direction undergoes the typical jump of the radial component due to the passage of the blade trailing vorticity (Jessup, 1989). This jump, which is modeled with no thickness according to the potential theory, is instead widespread over a finite thickness due to the viscosity of the fluid. An overview of the TKE distribution is shown in figure 6.

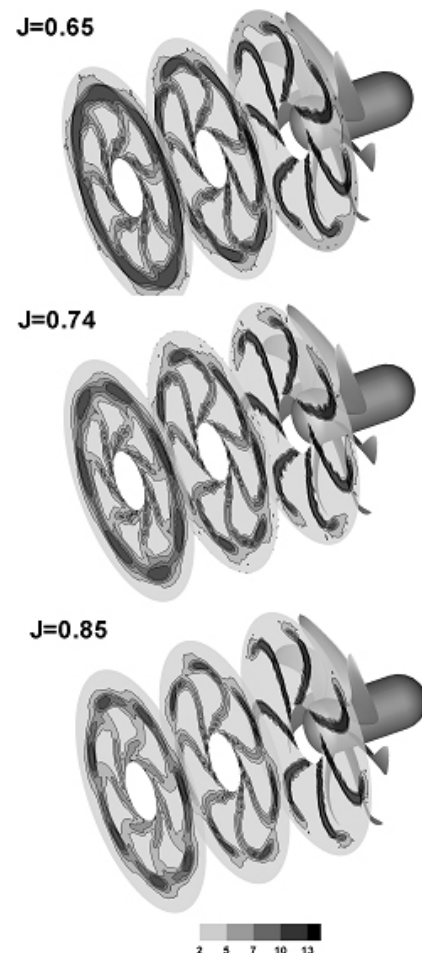


**Figure 6. Streamwise evolution of the turbulent kinetic energy (TKE) normalized with the average freestream kinetic energy (LDV measurements)**

This progressive bending of the blade wake is well described by the contour plots of the TKE (Figure 6). Actually, the turbulent wake is an effective indicator for the characterization of the trailing wake distortion. This distortion occurs with angular displacements between the tip vortex and the inboard blade wake which increase streamwise progressively. The general effect of the wake deformation is to stretch out the wake, moving the tip vortex further away from the inboard blade wake and possibly suppressing the roll-up.

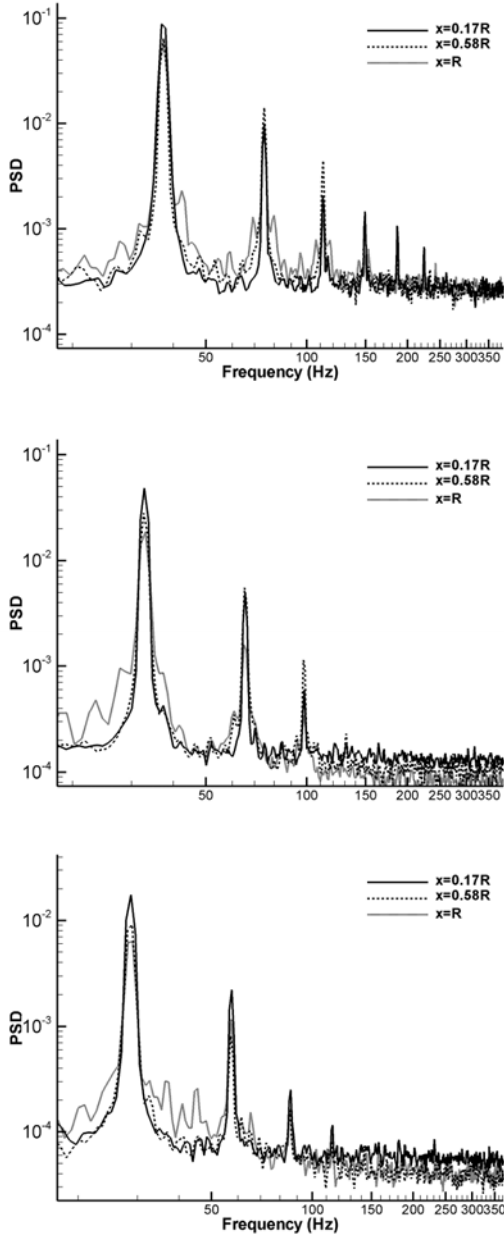


Figure 7. Power Spectral Density (PSD) of the velocity signals at  $J=0.65$  (top),  $J=0.74$  (mid) and  $J=0.85$  (bottom)

As the consequence of such a deformation, the wake of the actual blade starts to feel the action of the tip vortex of the previous one at a certain point, triggering a mechanism of mutual interaction between consecutive

spirals and causing the transition to instability of the propeller wake (Felli et al., 2006). The triggering position of such a mutual interaction depends strictly on the advance ratio, once fixed the propeller geometry, and tends to occur as closer to the propeller disk as the propeller load increases. In the present case, the iso-contours of the Turbulent Kinetic Energy (TKE) document this blade-to-blade interaction, being occurred in correspondence of the plane at  $x=R$ , independently of the advance ratio. In this region the trailing wake of the actual blade shows the tendency to lose the link with its tip vortex definitely and to be rolled up by the tip vortex of the previous blade.

Figure 7 describes the effect of the advance ratio and the streamwise distance on the Power Spectral Density (PSD) of the velocity signals, in the tip vortex. The power spectrum of the randomly acquired LDV signals was estimated using the direct transform method (Gaster and Roberts, 1977). The energy content of the velocity signals is concentrated at the blade frequency and its multiple-harmonics mainly. PSD at  $J=0.65$  exhibit the larger number of resolved harmonics (six harmonics for  $J=0.65$ , four harmonics for  $J=0.75$  and  $J=0.85$ ). Peak intensity at the blade frequency reduces at the increasing  $J$  and moving streamwise. The nature of such a phenomenon is due to the superposition of two effects basically:

- The effect of the turbulent diffusion that smoothes the velocity peaks in the tip vortex streamwise.
- The mechanism of instability involving a cascade energy transfer process from the blade to the shaft harmonic, according to Felli et al. (2006) and Felli et al. (2008). The occurrence of a modulation at the shaft frequency in the phase averaged velocity signals at  $x=R$  and  $J=0.65$  (Figure 8) as well as the appearance of some additional harmonics in the power spectrum seems to support this statement (Figure 7).

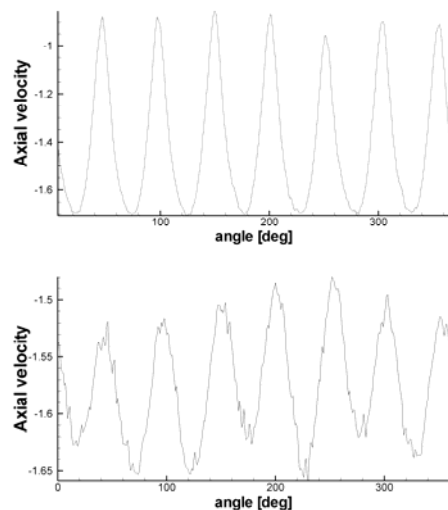
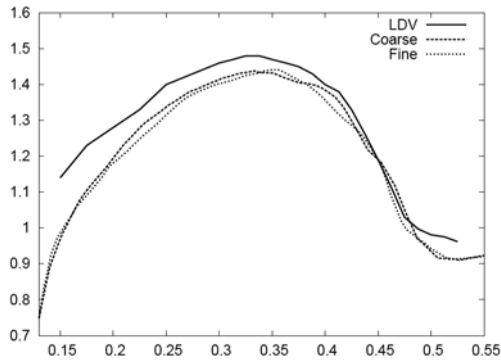


Figure 8. Angular evolution of the axial velocity in the tip vortex at  $x=0.17R$  (top) and  $x=R$  (bottom), for  $J=0.65$ .

## 6 CFD VALIDATION

In this section we make a qualitative and quantitative comparison of the experimental and computational results, with the aim of investigating and validating the accuracy of the LES results for the relevant flow features. As noted in section 5.1, the computational prediction of the thrust and torque is in good agreement, within 5% for all computed values, with the values obtained in the experiments. Below, we investigate the velocity field in the near wake. Due to space constraints, we can only include a small number of the comparisons which have been made. In fact, we restrict ourselves to the first LDV measurement plane at  $x = 0.17R$  and the intermediate advance number,  $J = 0.74$ .



**Figure 9.** The axial velocity, normalized with  $U_\infty$ , at  $x = 0.17R$ . On the horizontal axis is the normalized radius  $r/R$ . The radial line is chosen at an angle so that it passes in the middle between two blade wakes.

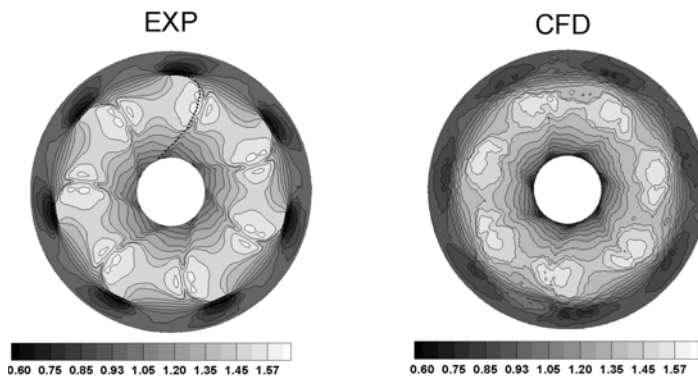


**Figure 10.** Experimental and computational analysis of the propeller wake at  $x=0.17R$  for  $J=0.74$ . The axial velocity normalized by  $U_\infty$  is shown.

In figure 9, we show a comparison of the axial velocity along a radial line. It is seen that the shape and width of the wake are well predicted. The maximum axial acceleration is slightly closer to the center line than  $r/R = 0.7$ , which is the location where the blades are designed to give maximum circulation. The experiments indicate a higher axial velocity in the inner region of the wake. For other line plots, cutting through areas with large gradients, the simulations generally give smoother curves than the experiments, and are not able to capture the sharpness of the flow structures. The location of the flow structures is however well predicted. These conclusions

are also supported by the 2D plot of the axial velocity in figure 10. We see that the location and overall strength of the wake are well predicted, while the flow features are more too "diffused" in the LES results. We also note that the blade wakes differ slightly between the different blades, for the LES results. At this station this is an artificial effect, probably caused by the fact that the grid is not exactly symmetric.

In general, for the velocity in the wake, the LDV measurements give a better resolution and accuracy than the LES in this study. With an improved mesh, with more cells, the LES results will naturally become more accurate. A principal advantage of the simulations, as compared to the experiments, is that the LES results contain the velocity/pressure field in the whole computational domain. Therefore it is possible to analyze the flow in regions with no optical access, or where it is difficult to measure for other reasons. Furthermore, since the three-dimensional velocity distribution is known, it is possible to perform other types of post-processing. This is exemplified in figure 11, with an iso-surface of the axial velocity which illustrates the spatial evolution of flow structures emanating around the blade tip.

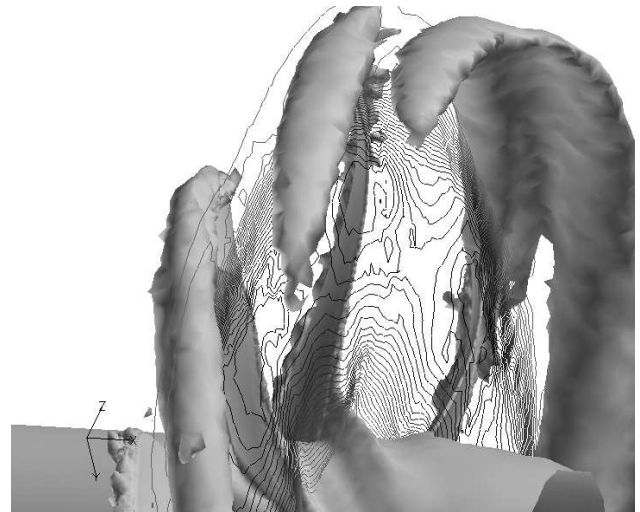


**Figure 11.** ( $J=0.74$ , LES) Iso-surface of the axial velocity and contour lines of the axial velocity on the plane  $x = 0.17R$ .

## 7 DISCUSSION AND CONCLUSIONS

The problem of the wake evolution and instability for a submarine propeller, running in open water conditions, was investigated in the present research activity. The study concerned velocity measurements by LDV phase sampling techniques and numerical simulation of the velocity/pressure field by LES.

On the physical side, the typical features of the propeller wake in the near field (e.g. streamtube contraction, roll up) as well as the effect of the loading conditions on the wake deformation and on the mechanisms of turbulent diffusion and instability inception were highlighted. In particular, it was observed that the transition to instability tends to occur closer to the propeller disk as to a

conventional propeller with a lower number of blades, the spiral-to-spiral distance being smaller. Furthermore, the occurrence of some additional harmonics in the power spectra of the velocity signals at the most downstream plane supports the results of literature concerning the transfers of energy in the transition wake (see Felli et al. 2006, Felli et al, 2008). In this regard, additional measurements focused on the analysis of the mechanisms of evolution of the tip vortex in the transition wake, as in Felli et al. (2008), are necessary to find out the nature of such additional harmonics.

For propeller simulations, it is possible to use software based on the boundary element method (BEM), the Reynolds averaged Navier-Stokes equations (RANS) and LES. The main motivation for the use of LES is for the investigation of large scale unsteady (in the rotating reference frame) effects. Examples of this include the following four situations. (1) Simulation of cavitation, see Bensow et al. (2008); (2) The propeller in crashback conditions; see e.g. Jang and Mahesh (2008); (3) The propeller in a non-uniform inflow; (4) The study of wake instability, as in the present paper. As noted in section 6 however, the mesh resolution and distribution is not sufficient to investigate the wake structure, where the instability sets in, with sufficient accuracy. With a suitable distribution of computational cells, this may be accomplished with 10-20 million cells. This estimate is based on the experience gained from the computations presented in this paper. In general, submarine propellers put more severe requirements on the computational mesh than conventional propellers. The main reason for this is the design which results in weaker flow structures, which in turn are more easily dissipated artificially when the mesh is too coarse. Submarine propellers also have more blades, and therefore require the corresponding increase in number of cells in the mesh, to resolve the geometric detail.

Comparisons between flow field LES predictions and LDV measurements revealed a good agreement concerning both thrust and torque coefficients and location and general wake strength. The sharp flow features, including blade wakes and tip vortices, are however dissipated artificially and a finer mesh is required to study the wake dynamics, and the associated wake instability.

## REFERENCES

Bensow, R. E. and Liefvendahl, M. (2008). Implicit and explicit subgrid modeling in les applied to a marine propeller.(AIAA-2008-4144).

Bensow, R. E., Huuva, T., Bark, G., and Liefvendahl, M. (2008). Large Eddy Simulation of Cavitating Propeller Flows. In 27th Symposium on Naval Hydrodynamics, Seoul, Korea.

Bensow, R. E., Liefvendahl, M., and Wikström, N. (2006). Propeller Near Wake Analysis Using LES With a Rotating Mesh. In 26th Symposium on Naval Hydrodynamics, Rome, Italy.

Cenedese A., Accardo L., Milone, R. (1985). Phase sampling in the analysis of a propeller wake, International Conference on Laser Anemometry Advances and Application, Manchester, UK.

Di Felice F, Di Florio D, Felli M, Romano G.P. (2004). Experimental Investigation of the Propeller Wake at Different Loading Conditions by Particle Image Velocimetry. Journal of Ship Research.Vol.48, N.2, 168-190.

Felli M., Di Felice F. (2005). Propeller wake analysis in non uniform inflow by LDV phase sampling techniques, Journal of Marine Science and Technology, Vol.10, N.4, pp.159-172.

Felli M., Di Felice F., Guj G., Camussi R. (2006). Analysis of the propeller wake by pressure and velocity phase measurements, Experiments in Fluids, N.1.

Felli M., Di Felice F. (2008). Characterization and modulation of the acoustical signature of a marine propeller operating in open water and in behind condition, Exponaval 2008, Vina De Mar, Chile.

Felli M., Guj G., Camussi R. (2008). Effect of the number of blades on propeller wake evolution, Experiments in Fluids, N.44.

Gaster M., Roberts J.B. (1977). The spectral analysis of randomly sampled records by a direct transform, Proceedings Royal Society London, A 354, pp.27-58.

Jang, H. and Mahesh, K. (2008). Large Eddy Simulation of Ducted Propulsors in Crashback. In 27th Symposium on Naval Hydrodynamics, Seoul, Korea.

Jessup S. (1989). An experimental investigation of viscous aspects of propeller blade flow, The Catholic University of America, Washinngton DC.

Kerwin J.E. (1986). Marine propellers, Annual review of fluid mechanics, Vol.18, pp.367-403.

Schumann, U. (1975). Subgrid scale model for finite difference simulation of turbulent flows in plane channels and annuli. J.Comp.Phys., 18(4):376-404.